ACS APPLIED MATERIALS & INTERFACES

Research Article

www.acsami.org

Facile Route for the Synthesis of a Vertically Aligned ZnO–PANI Nanohybrid Film for Polyphenol Sensing

Jagvir Singh,*[,†] Amol Purushottam Bhondekar,[†] Madan Lal Singla,[†] and Anupama Sharma[‡]

[†]Council for Scientific and Industrial Research (CSIR), Central Scientific Instruments Organisation (CSIO), Sector 30C, Chandigarh 160030, India

[‡]UICET, Panjab University, Chandigarh 160014, India

Supporting Information

ABSTRACT: Vertically aligned zinc oxide (ZnO) nanorods have been fabricated on a polyaniline (PANI) film template after electrochemical seeding and hydrothermal growth in a nutrient medium at a low temperature of 65 °C. Dense *c*-oriented [0001], hexagonal-shaped, vertically aligned ZnO nanorods are obtained on the PANI film surface, which is confirmed by X-ray diffraction and scanning electron microscopy studies. The nanohybrid film used as the working electrode has been characterized for sensing catechin polyphenol in different tea varieties through cyclic voltammetry. Principal component analysis shows enhancement in the classification ability of the nanohybrid film for various concentrations of catechin standard and tea infusions.

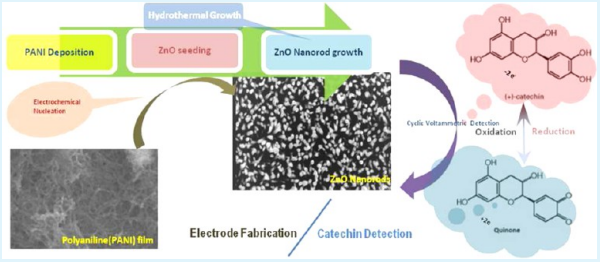

KEYWORDS: *vertically aligned ZnO nanorods, zinc oxide–polyaniline hybrid film, cyclic voltammetry, polyphenol, principal component analysis*

1. INTRODUCTION

Zinc oxide (ZnO) is a direct-band-gap (E_g = 3.37 eV) semiconductor with a large exciton binding energy (60 meV),[1,2] exhibiting near-UV emission, transparent conductivity, and piezoelectricity. Because morphologies have been correlated with optical and electrical properties, there has been intensive focus on fabricating 1D ZnO nanostructures.[3−6] Various kinds of ZnO nanostructures have been realized, such as nanodots, nanorods, nanowires, nanobelts, nanotubes, nanobridges and nanonails, nanowalls, nanohelixes, seamless nanorings, mesoporous single-crystal nanowires, and polyhedral cages.[7−9] Among the 1D nanostructures, ZnO nanorods and nanowires have been widely studied because of their easy nanomaterial formation and device applications.

There has always been a challenge in synthesizing vertically aligned ZnO nanorods, which have important applications in sensor development. It has been widely reported that control over the dimension, composition, position, and orientation of the ZnO nanostructures plays a very crucial role in the development of novel devices.[10,11] Various techniques, viz., radio-frequency magnetron sputtering,[12] metal−organic chemical vapor deposition,[13] spray pyrolysis,[14] pulsed-laser deposition,[15] and continuous-spray pyrolysis (CoSP),[16] are being used to achieve orientation for ZnO nanorods. Most of these methods require harsh reaction conditions such as high temperature and low or high pressure, seriously restricting the large-scale production and escalating the cost of production. In contrast, the solution methods for oriented nanorods involve low-cost procedures with moderate conditions. Also, because the orientation of the nanorods plays a major role in sensor device applications, it can be achieved through the formation of a hybrid film by solution methods. Controlling the size and shape of ZnO nanorods in the hybrid film provides a better mode for investigating the dependence of the electronic and optical properties on the size confinement and dimensionality.[17] Among all of the structures, vertically aligned ZnO nanorods would offer the unique opportunity to modulate the physical properties by changing the aspect ratio of ZnO nanorods. Various efforts have been made to fabricate vertically aligned ZnO nanorods at lower temperatures.[18] The direct growth of vertical ZnO nanowires and nanorods on metal and other substrates has recently been reported to reduce the interfacial resistance.[19] Electrochemical deposition is a considerably promising approach for growing nanomaterials because of its low cost, large-scale production, and low-temperature growth.[20,21]

Accurate analysis of polyphenols is crucial for tea characterization. The major polyphenolic compounds in tea belong to the catechin family, contributing up to 30% of the tea solids by weight depending upon the manufacturing practice. Important contributions have been made toward analysis of catechins, caffeine, and gallic acid in the tea samples through high-performance liquid chromatography (HPLC) optimization.[22] Vast amounts of work have been done toward e-nose and e-tongue development for tea and beverage analysis such as a tin oxide based electronic nose by Dutta et al.,[23] electronic-nose-

Received: April 12, 2013
Accepted: May 21, 2013
Published: May 21, 2013

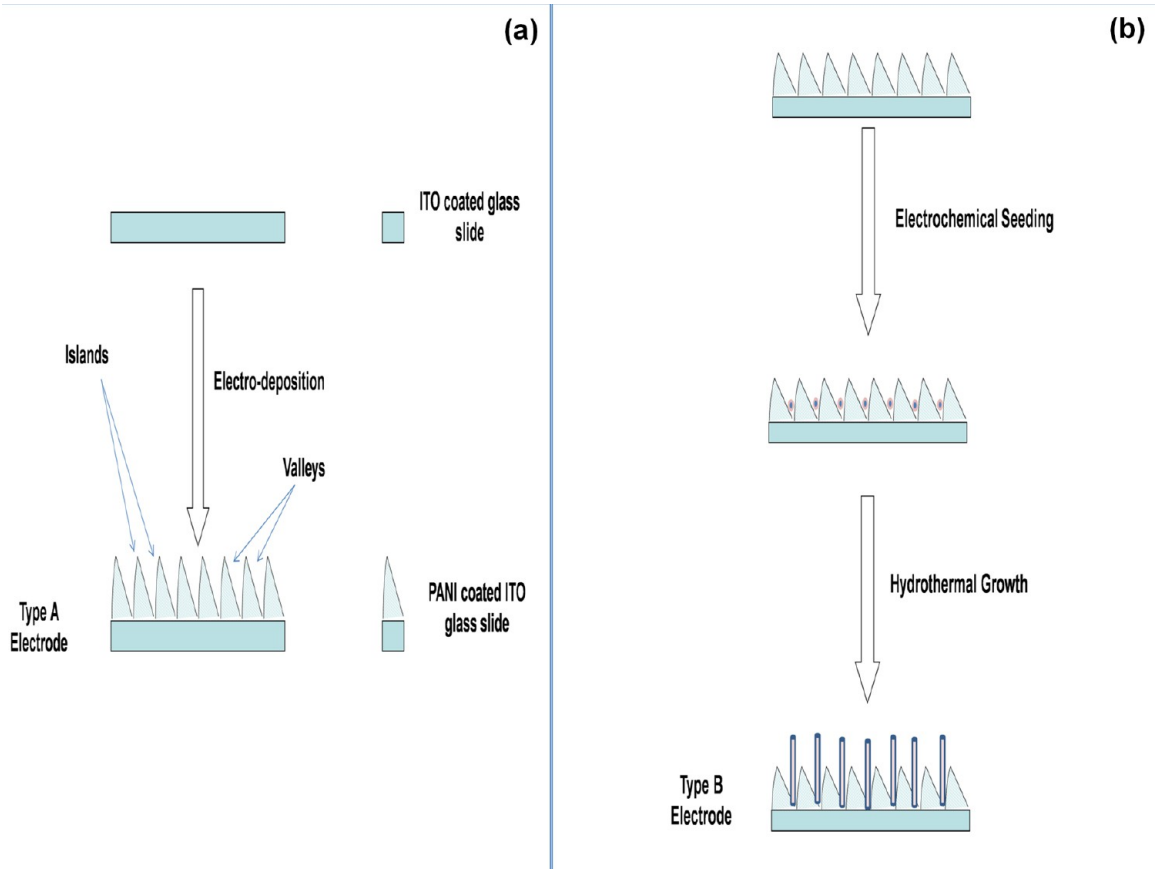

Figure 1. Schematic diagram for the fabrication of type (a) A and (b) B electrodes.

based identification of wine aromas by Lozano et al.,[24] electronic nose for black tea classification and for black tea fermentation monitoring by Bhattacharyya et al.,[25,26] and tea quality standardization through an electronic nose by Dutta et al.[27] Cyclic voltammetry (CV) is among the most commonly reported electrochemical characterization of tea.[28,29] The polyphenols in the tea samples are readily oxidized and reduced reversibly during CV analysis. Sensor selectivity studies are crucial for the application of CV as an analytical tool. The selectivity is influenced by the electronic flow at the working electrode. The redox behavior of the nanohybrid layer is dependent upon the layered arrangement of the nanofilm and inherent electrochemically induced electronic properties, as a consequence of the ion-exchange properties resulting in a change in the CV response observed.[30] Besides depending upon the rate and range of the potential scan, the CV response is dependent upon the electronic properties of the working electrode, which is further dependent upon its surface characteristics. The change in the CV response of the working electrode can be induced by the formation of a nanohybrid film on the conducting surface provided by an indium−tin oxide (ITO) layer on the glass surface. This CV response has been exploited for characterizing the sensor selectivity for various tea samples, which in itself is a novel approach. A ZnO-based (inorganic−organic) hybrid film-coated electrode has been studied using CV to detect the biomolecules dopamine, ascorbic acid, and uric acid.[31] Hybrid materials have been previously employed as the coating materials for gas-sensing arrays.[32] It involved a comparison of the calibration data from various analyses of standard gases. Pattern recognition methods such as principal component analysis (PCA) and hierarchical clustering have been applied to determine possible gas-coating interaction mechanisms and the potential selectivity of a given array.[33] Pattern classification has been done after dimensionality reduction and support vector machines using PCA for application in an electronic tongue.[34−37]

The present work involves the fabrication of vertically aligned ZnO nanorods in the first step after electrochemical nucleation on the PANI film. After fabrication, the obtained nanohybrid film has been used for electrochemical sensing of the catechin polyphenol using a three-electrode system. The method used for the synthesis for aligned nanorods, besides being cost-effective, provides a unique opportunity for the synthesis of ZnO nanorods with tunable morphology.

2. EXPERIMENTAL SECTION

2.1. Materials. All of the chemicals used in the experiments were AR-grade reagents. Aniline was supplied by Spectro Chem Pvt. Ltd., India, hexamine and HCl by S.D. Fine Chemicals, India, and $Zn(NO_3)_2$ by Loba Chemie Pvt Ltd., India. Pt and Ag−AgCl reference electrodes were supplied by CH Instruments (Austin, TX). Catechin and ITO-coated slides were supplied by Sigma Aldrich and had sheet resistances of 8−12 Ω/sq.

Two types of black tea samples were used in the study based upon their manufacturing methods, namely, Cut-Tear-Curl (CTC) and orthodox methods. These samples were deliberately chosen to obtain maximum variability in the catechin concentrations because the catechin concentrations are significantly higher in orthodox teas than CTC teas. In India, two varieties of teas, namely, *Camellia sinensis* var. *assamica* and *Camellia sinensis* (L.) O. Kuntze, are grown, and CTC and orthodox methods respectively are used to manufacture black teas. The samples of CTC tea were procured from the local market, while

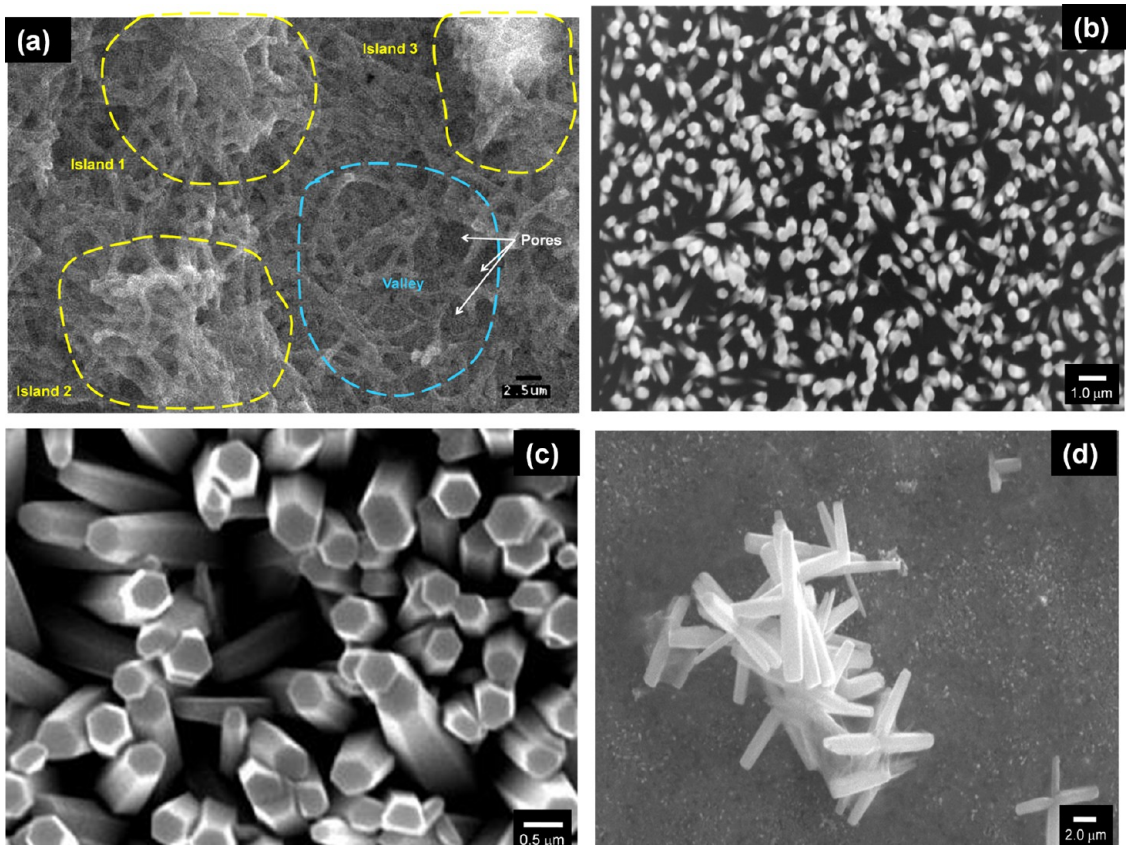

Figure 2. SEM images of (a) the PANI film over an ITO-coated glass slide, (b and c) ZnO nanorods on the PANI film over an ITO-coated glass slide, and (d) ZnO nanorods grown on a bare ITO glass slide.

orthodox tea was sourced from the Institute of Himalayan Bioresource Technology, Palampur (a constituent laboratory of CSIR).

2.2. Preparations of Tea Infusion and Catechin Samples. *Tea Infusion.* To prepare a tea infusion, 0.4 g of a tea sample was added to 20 mL of boiling water in a 400 mL beaker and stirred with a magnetic stirbar for 10 min. The tea extract was then cooled to room temperature and filtered on a Whatman Filter No. 40. Two concentrations of samples were prepared for CV analysis by diluting the extract 10 and 20 times, respectively, in a phosphate buffer [65% (w/v) 50 mM disodium hydrogen phosphate and 35% (w/v) 50 mM sodium dihydrogen phosphate] at pH 7.0. The samples were prepared in quadruplicate.

Catechin Samples. Two concentrations, 0.1 and 0.2 mM, of catechin were prepared in a phosphate buffer [65% (w/v) 50 mM disodium hydrogen phosphate and 35% (w/v) 50nM sodium dihydrogen phosphate] at pH 7.0. The samples were prepared in quadruplicate.

2.3. Hybrid Film Synthesis. Two types of film-based electrodes were fabricated from the pretreated ITO-coated glass slides (treated for 15 min each with acetone, isopropyl alcohol, and ethanol in the same sequence). The first type of electrode (named type A) was prepared by electrodepositing PANI on an area of 1 cm^2 on an ITO-coated glass slide. PANI was potentiostatically deposited by applying a potential of +0.744 V for 10 min in a 10 mL aqueous solution of 0.5 M HCl and 91 μL of an aniline monomer using a three-electrode system, where Pt wire was used as the counter electrode, saturated Ag–AgCl as the reference electrode, and the ITO-coated glass slide as the working electrode at room temperature. The films were washed two or three times with deionized water and dried in air. The schematic diagram is given in Figure 1a.

The second type of electrode (named type B) was obtained from a type A electrode by a two-step process, as shown in Figure 1b. The first step involved electrochemical seeding of ZnO on the PANI film. This was again done by a three-electrode system as mentioned earlier except that the working electrode now was the type A electrode obtained previously. The galvanostatic process was applied to deposit the seed layers, which acted as the nucleation source for the subsequent growth of ZnO nanorods. The current density used for seed-layer deposition was −1.30 mA/cm^2, and the deposition time was 120 s in the electrolytic solution, which was an aqueous solution of 0.1 M $Zn(NO_3)_2$. Hydrothermal growth of ZnO nanorods was carried out in the electrolytic solution composed of aqueous 0.1 M $Zn(NO_3)_2$. The process of hydrothermal growth consisted of immersion of the modified substrate, i.e., a PANI film electrochemically seeded with ZnO nanoparticles on the ITO glass slide, into the electrolyte contained in a sealed beaker for a period of 2 h with the temperature maintained at 65 °C. The schematic diagram is given in Figure 1b. For each type of electrode, 24 numbers were fabricated.

3. CHARACTERIZATION

3.1. Surface Morphology. Morphology studies of the air-dried PANI and PANI–ZnO hybrid films were carried out using a field-emission scanning electron microscope (Hitachi S4300 SE/N) operated at 15 kV under a vacuum of 40 Pa. Interspersed fibers of polyaniline were observed in the PANI film. A surface view of the PANI–ZnO hybrid film showed well-aligned ZnO nanorods of almost uniform diameter in the range of 300–400 nm.

3.2. Thickness. The thickness of the hybrid film was measured through a near-field scanning optical microscope of Park System, Korea, make (model XE-NSOM) and confirmed through an ellipsometric study of the films on an ellipsometer from J. A. Woollam, USA (model ESM-300). Both instruments gave a thickness of the PANI film in the range of 200–400 nm, indicating the depth of valleys in the PANI film around 200 nm.

dx.doi.org/10.1021/am401257q | ACS Appl. Mater. Interfaces 2013, 5, 5346–5357

3.3. Optical Properties. UV−visible spectra of pristine PANI fiber and a ZnO−PANI hybrid film deposited on ITO were observed in the range of 300−800 nm at room temperature on a UV−visible spectrophotometer (Perkin-Elmer Lambda 35). Pristine PANI showed two prominent absorption peaks at 360 and 427 nm and a broad band between 600 and 800 nm.

The X-ray diffraction data for prepared samples were recorded on a Panalytical X'Pert Pro diffractometer with Cu Kα radiation (λ = l.5418 Å) over the range of $10° < 2\theta < 90°$ under ambient conditions.

Fourier transform infrared (FTIR) spectra of pure PANI and a PANI−ZnO composite in KBr were carried out in the frequency range of 500−4000 cm^{-1} on Perkin-Elmer RX-1 FTIR spectrophotometer.

3.4. Electrochemical Properties. The electrochemistry was carried in an Electrochemical Workstation from CH Instruments, USA (model 660C), using a conventional three-electrode cell. The reference electrode was Ag|AgCl/KCl_{sat}, and platinum was used as the counter electrode. For comparative analysis, three types of working electrodes were used, viz., type A, type B, and an ITO-coated glass slide. Six CV cycles were run per sample per electrode at a scan rate of 25 mV s^{-1} from −0.1 to +0.4 V. A fresh electrode was used for each analysis. Thus, a total of 24 electrodes of each type were used.

In the present study, the second CV cycle out of six CV cycles was chosen for data analysis at a constant temperature and pH. It was observed that the first cycle gave inconsistent results. Also, various scan rates, viz., 5, 10, 15, 25, 50, and 100 mV s^{-1}, were tried. With the current peak intensity being maximum at 25 mV s^{-1}, it was chosen as the scan rate for all other experiments.

3.5. Chemometrics. In order to visualize the discrimination capabilities of the three electrodes, PCA was done. PCA is a mathematical procedure that uses an orthogonal transformation to convert a set of observations of possibly correlated variables into a set of values of linearly uncorrelated variables called principal components. It provides an informative representation of original data with lower dimensions. Usually, the first two principal components (PC1 and PC2) map the maximum variance and information of the input data. The *Unscrambler 9.1* (CAMO, Norway) software was used for PCA. The CV data of each type of electrode at each sample were averaged, thus obtaining four instances of readings for each electrode. The values of the currents at each potential point of the CV scan (forward and reverse) were treated as features and arranged in columns. Thus, a data matrix of 72 rows (i.e., observations) by 1000 columns (i.e., features) was obtained. These data were mean-centered and scaled prior to PCA.

4. RESULTS AND DISCUSSION

Figure 2a, the scanning electron microscopy (SEM) image, shows the surface morphology of a PANI film over an ITO glass slide. Interspersed PANI fibers with "islandic" (enclosed by yellow dotted lines) morphology can be observed. Each "island" consists of several branched structures surrounded by "valleys" (enclosed by blue dotted lines). The height profile obtained by near-field scanning optical microscopy confirms the height and depth of the PANI film as 400 and 200 nm, respectively. It is observed that the fiber density on the islands is more compared to the valleys, and significant numbers of pores are visible in the valley region. These pores provide templates for subsequent hydrothermal growth of the ZnO

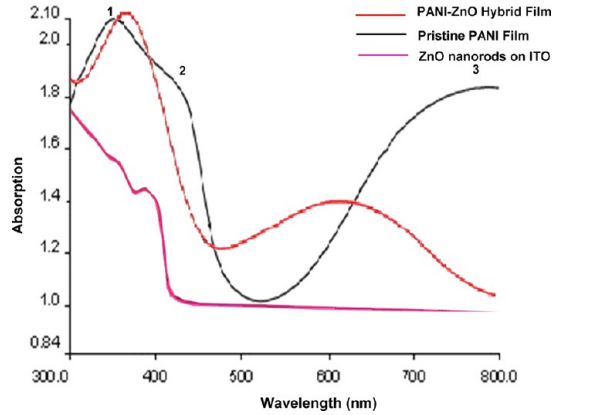

Figure 3. UV−visible absorption spectra of PANI, the PANI−ZnO film, and ZnO nanorods on ITO.

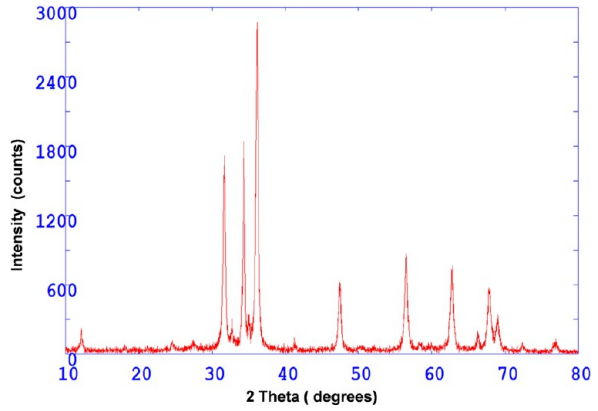

Figure 4. XRD spectra of ZnO−PANI.

nanorods, resulting in a type B electrode.[38,39] This morphology helps to obtain vertically aligned ZnO nanorods over the surface of the PANI film.

Parts b and c of Figure 2 show the surface morphology of the grown ZnO nanorods over the PANI surface. Figure 2c has higher magnification than Figure 2b. ZnO nanorods with a hexagonal cross section are visible, exhibiting good vertical alignment. Growth kinetics of nanocrystals is popularly explained by the diffusion-limited Ostwald ripening process following the Lifshitz−Slyozov−Wagner (LSW) theory.[40,41] Numerous researchers have explained the diffusion-controlled growth of the crystals: Qu et al.[42] for the growth of CdSe nanocrystals, Oskam et al.[43] for TiO_2 crystals, and El-Sayed et al.[44] for gold nanoparticles. However, here the simple diffusion-limited Ostwald ripening model cannot explain the 0.8−1.0-μm-sized nanorods with average diameter of around 180 nm. It is possible only if the growth is guided by diffusion of the particles as well as reaction at the surface, which is supported by the theoretical considerations.[45] ZnO with a polar hexagonal wurzite structure can be ascribed to the hexagonal close packing of oxygen and zinc atoms, their spatial arrangement (in point group 3*m* and space group *P*63*mc*), and the presence of zinc atoms at the tetrahedral sites. Thus, the crystal habit of wurzite ZnO exhibits well-defined crystallographic faces, i.e., polar-terminated (0001) planes and six side facets, which are generally bound by the $(10\bar{1}0)$ family of planes. The growth rates of different families of planes follow the sequence (0001) > $(10\bar{1}1)$ > $(10\bar{1}0)$.[46] ZnO anisotropic structures are normally

dx.doi.org/10.1021/am401257q | ACS Appl. Mater. Interfaces 2013, 5, 5346−5357

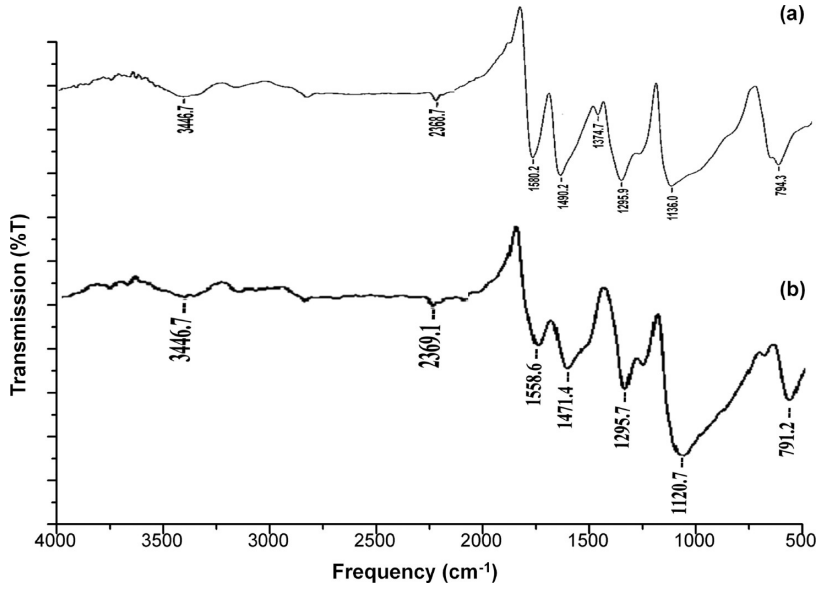

Figure 5. FTIR spectra of (a) PANI (b) the PANI–ZnO film.

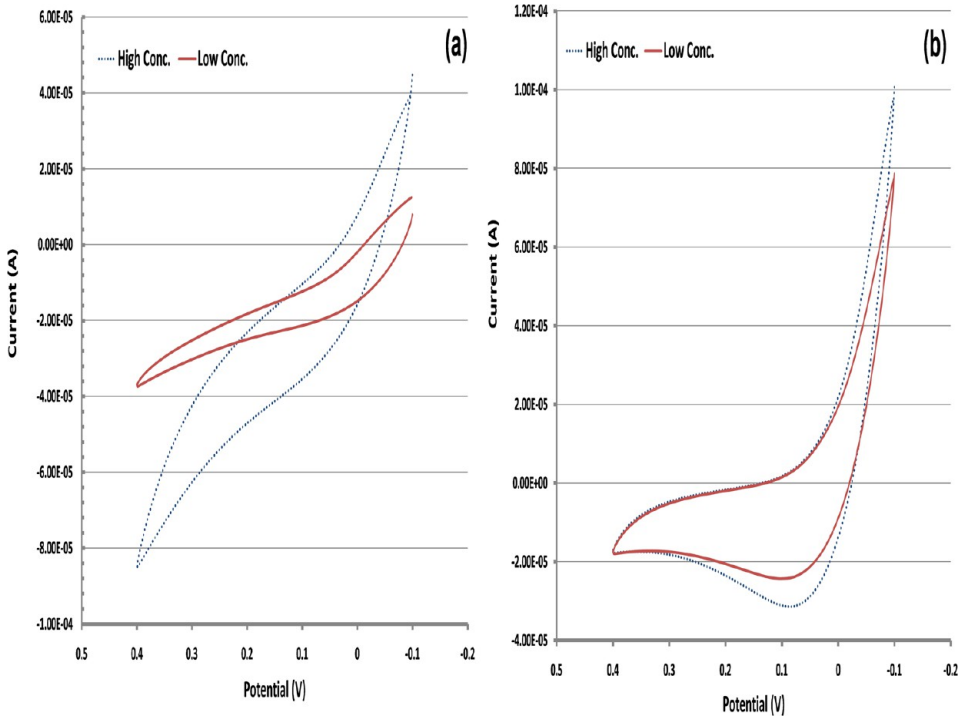

Figure 6. Cyclic voltammograms of catechin standards on type (a) A and (b) B electrodes.

bound by six $(10\bar{1}0)$ facets grown along the (0001) direction, i.e., along the *c* axis of the rods.

If the diffusion-limited Ostwald ripening according to the LSW theory[40,41] were to be the sole contributor of the growth mechanism, then the rate law would be given by

$$L^3 - L_0^3 = Kt$$

where L is the average length at time t and L_0 is the average initial length of the nanorods. The rate constant K is given by

$$K = \frac{8\gamma D V_m^2 C_\infty}{9RT}$$

The pores present the templates for initial seeding, whereas the growth of the nanorods mainly occurs by the diffusion of monomers from solution to the nanorod surface or by reaction at the surface where units of diffusing particles get assimilated into the growing nanorods. Therefore, diffusion and surface reactions are two limiting cases in the growth of nanorods. In the presence of PANI fibers, the nanorod growth is essentially controlled by diffusion. The PANI fibers present a barrier to the diffusion of monomers to the nanorod surface because of which the contribution of the surface reaction becomes more prominent. Thus, the growth of nanorods occurs through a combination of diffusion and surface reaction processes. The PANI fibers appear to selectively cap the side facet of the ZnO

Scheme 1. Two-Step Oxidation of Catechin

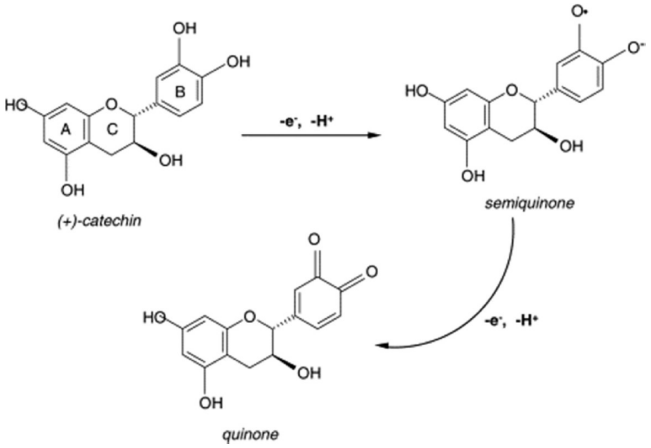

nanorods, allowing the growth to occur selectively along the *c* direction and resulting in vertically aligned nanorods.

They have relatively uniform size with an average diameter of 180 nm. Therefore, the PANI template has been able to induce growth along the vertical axis for the ZnO nanorods. In order to assert the vertical growth and compare ZnO nanorods on a bare ITO surface as well (the SEM image for the same is given in Figure 2d), a haphazard growth of ZnO nanorods is evident because of the absence of porous templates.

UV−visible spectra of a pristine PANI fiber and a ZnO−PANI hybrid film deposited on ITO were recorded in the wavelength range of 300−800 nm and are shown in Figure 3. In the UV−visible spectrum of pristine PANI (black curve), two prominent absorption peaks were observed at 360 and 427 nm. This confirms the presence of polaron and/or bipolaron levels involving the valence and conduction bands. The 360 nm band is attributed to the p−p* transition in the benzoid ring. The peak at 430 nm is attributed to protonation of polyaniline (polaron and bipolaron), indicative of the conducting state. A broad band between 500 and 800 nm is observed and is due to excitation of the quinoid ring corresponding to the semiconducting phase of PANI−$HClO_4$ nanorods (Emraldine Salt-ES).[47] A peak at 360 nm (red curve) is the characteristic band of the wurtzite hexagonal pure ZnO. The absence of any other bands in the spectrum confirms that pure ZnO has been synthesized.

If we compare the UV−visible spectra of a PANI−ZnO hybrid film and pristine PANI, it could be seen that the shapes of the peaks are very similar, but some shifting in the bands is noticed. In the case of the hybrid film, the peak 1 almost retains its position with a slight red shift, while peak 2 disappears.

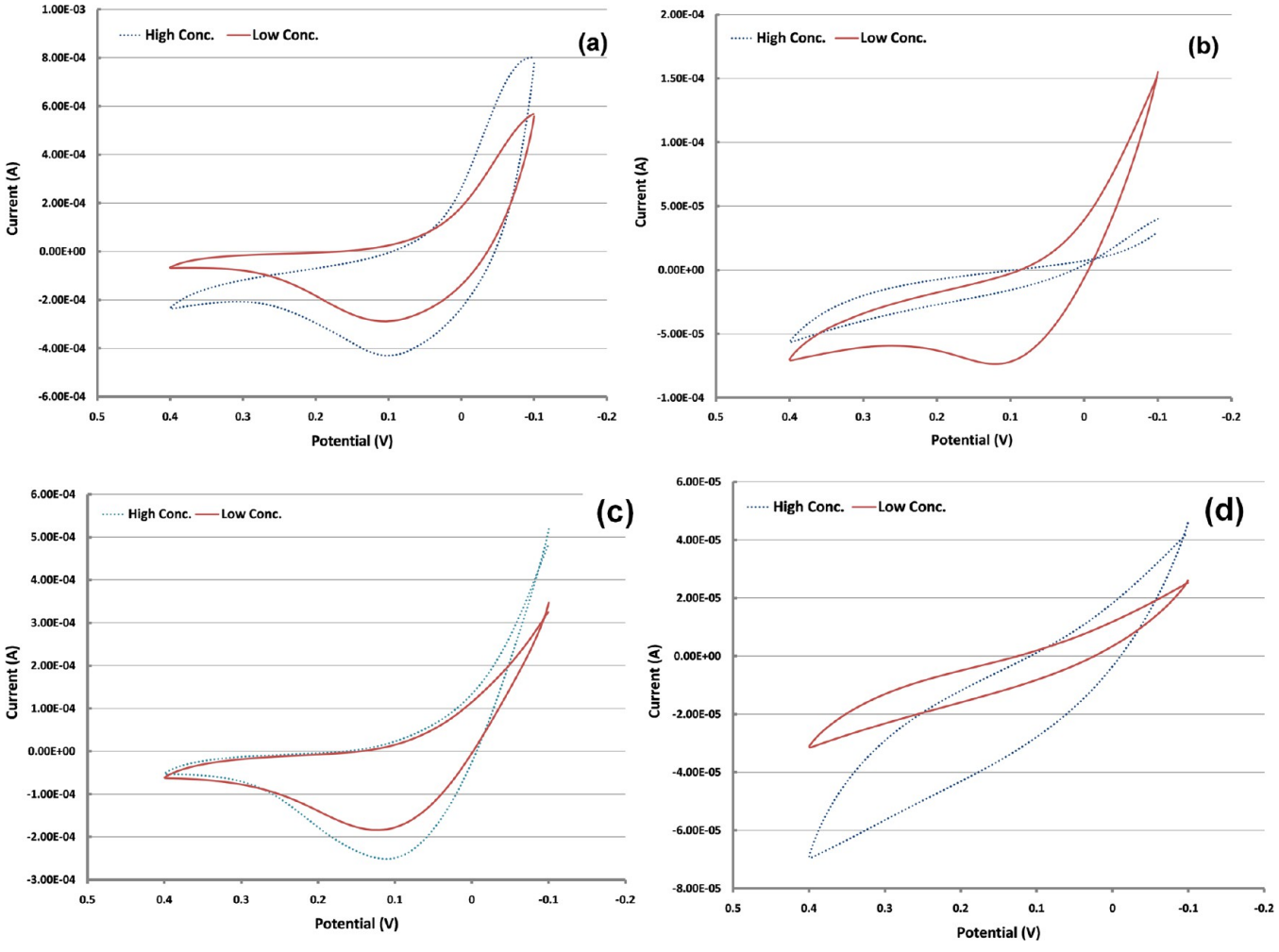

Figure 7. Cyclic voltammograms of tea infusions at two dilutions: (a) CTC on a type A electrode; (b) CTC on a type B electrode; (c) orthodox on a type A electrode; (d) orthodox on a type B electrode.

dx.doi.org/10.1021/am401257q | ACS Appl. Mater. Interfaces 2013, 5, 5346−5357

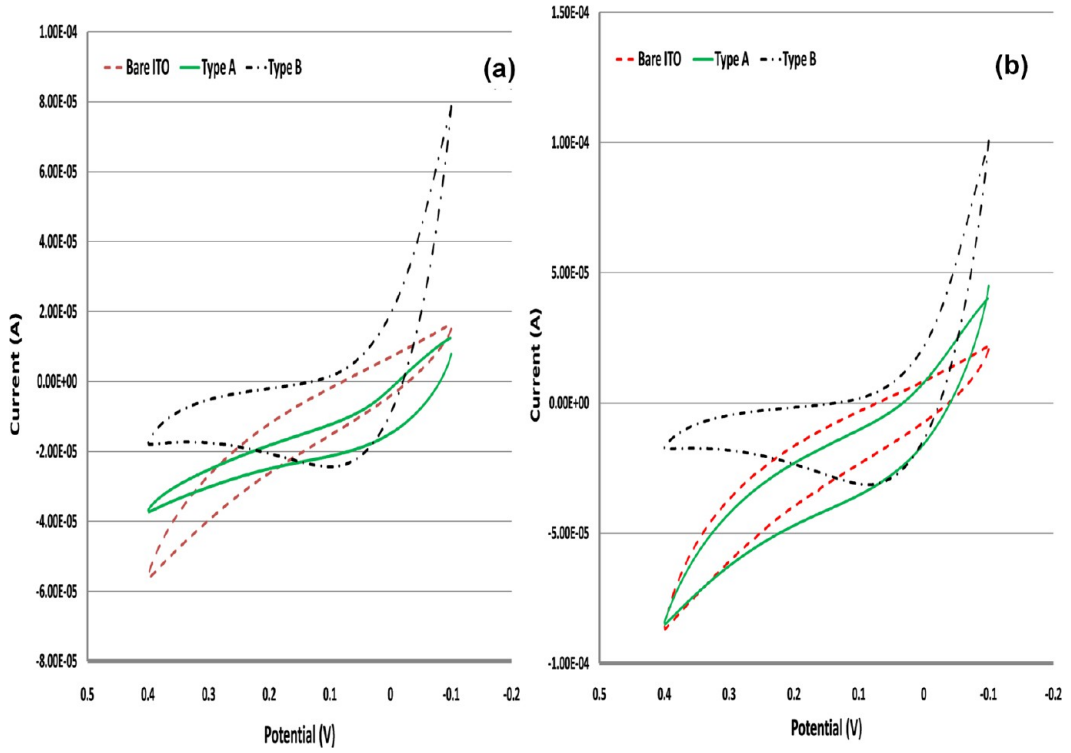

Figure 8. Cyclic voltammograms of catechin standards on three electrodes for (a) 0.1 mM and (b) 0.2 mM catechin.

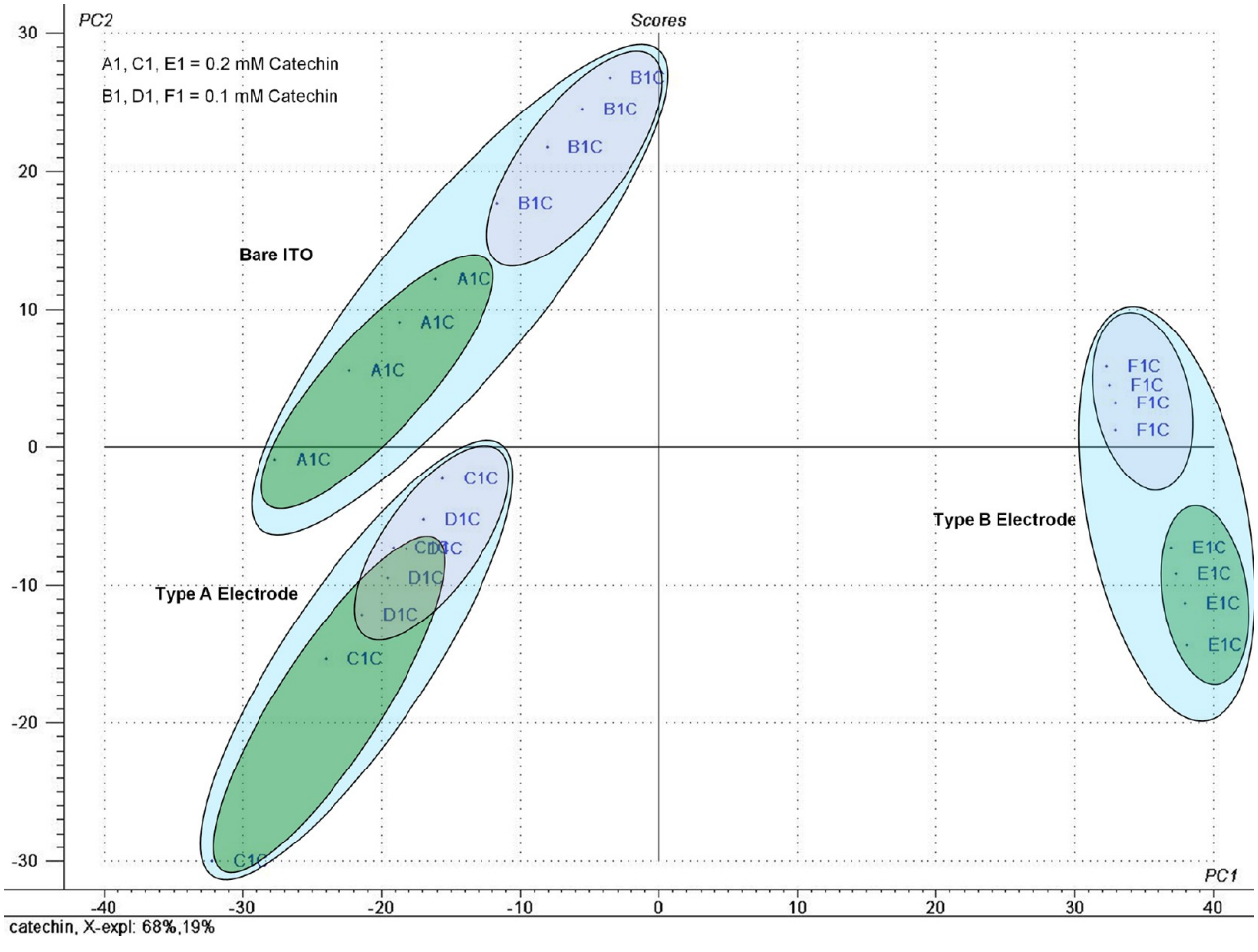

Figure 9. PCA plot of catechin with three types of electrodes.

dx.doi.org/10.1021/am401257q | ACS Appl. Mater. Interfaces 2013, 5, 5346−5357

Table 1. Biochemical Constituents of Tea Found by HPLC and UV−Visible Spectrosopy

	orthodox tea	CTC tea
3,5-dihydroxybenzoic acid (DBA)	0.487	0.451
gallic acid (GA)	0.848	0.760
catechin (C)	0.491	0.436
epigallocatechin gallate (EGCG)	6.010	1.593
epicatechin gallate (ECG)	1.337	0.684
caffeine (CAF)	3.130	4.277
theaflavins (TF)	0.147	0.622
thearubigins (TR)	5.050	12.647

Selective interactions between ZnO and the quinoid ring of ES, facilitate charge transfer from the quinoid unit of ES to ZnO via highly reactive imine groups, resulting in a considerable large blue shift in peak 3. Also, the interaction between the ZnO nanoparticles and PANI molecules results in an increased relative intensity of the peak for the PANI−ZnO hybrid film. The strong guest−host interactions in organic/inorganic composites take place because of hydrogen bonding in the form of NH (PANI)···O−metal (metal oxide), for example, NH···O−Ti in PANI/TiO_2.[48] The interaction between ZnO and PANI contributes to the decrease in the degree of orbital overlap between the π electrons of the phenyl rings with the lone pair of the nitrogen atom in the PANI molecules, which results in the formation of strong hydrogen bonding between them. This leads to a decrease in the extent of conjugation of PANI, thus resulting in an increased intensity of the peak in the PANI−ZnO hybrid film. Conclusively, absorption of the hybrid film increases over the whole range of visible light, indicating that electrophoretic deposition is effective in broadening the absorption of ZnO to the visible light range.

Figure 4 shows the XRD patterns of ZnO−PANI deposited films. The sharp intense peaks of ZnO confirm the good crystalline nature of ZnO. All peaks can be well indexed to the zincite phase of ZnO (International Center for Diffraction Data, JCPDS 36-1451). No peaks from other phases of ZnO and impurities are observed in the pattern of simple ZnO nanoparticles, suggesting that high-purity ZnO be obtained.

FTIR spectra of pure PANI and PANI−ZnO composite in KBr are given in Figure 5. The characteristic peaks of PANI at 791.2, 1120.7, 1295.7, 1471.4, 1558.6, 2369.1, and 3446.7 cm^{-1} correspond to the C═N iminoquinone, C═C stretching mode of the quinoid rings, the C═C stretching mode of the benzenoid rings, the stretching mode of C−N, and the stretching mode of N═Q═N, where Q represents the quinoid ring and the C−H bonding mode of the aromatic rings. The PANI−ZnO composite also shows the same characteristic

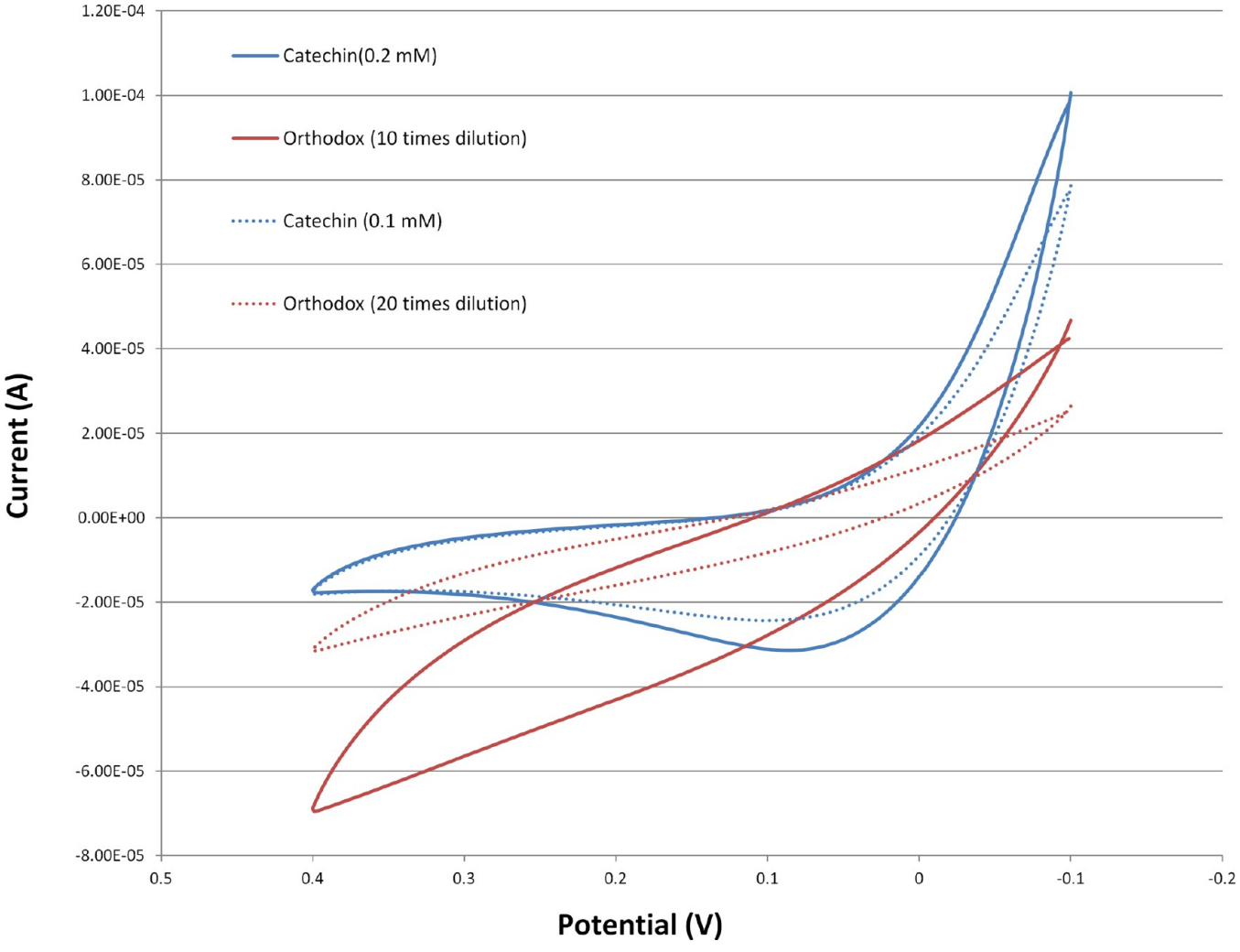

Figure 10. Cyclic voltammograms of catechin and orthodox teas on the type B electrode.

dx.doi.org/10.1021/am401257q | ACS Appl. Mater. Interfaces 2013, 5, 5346−5357

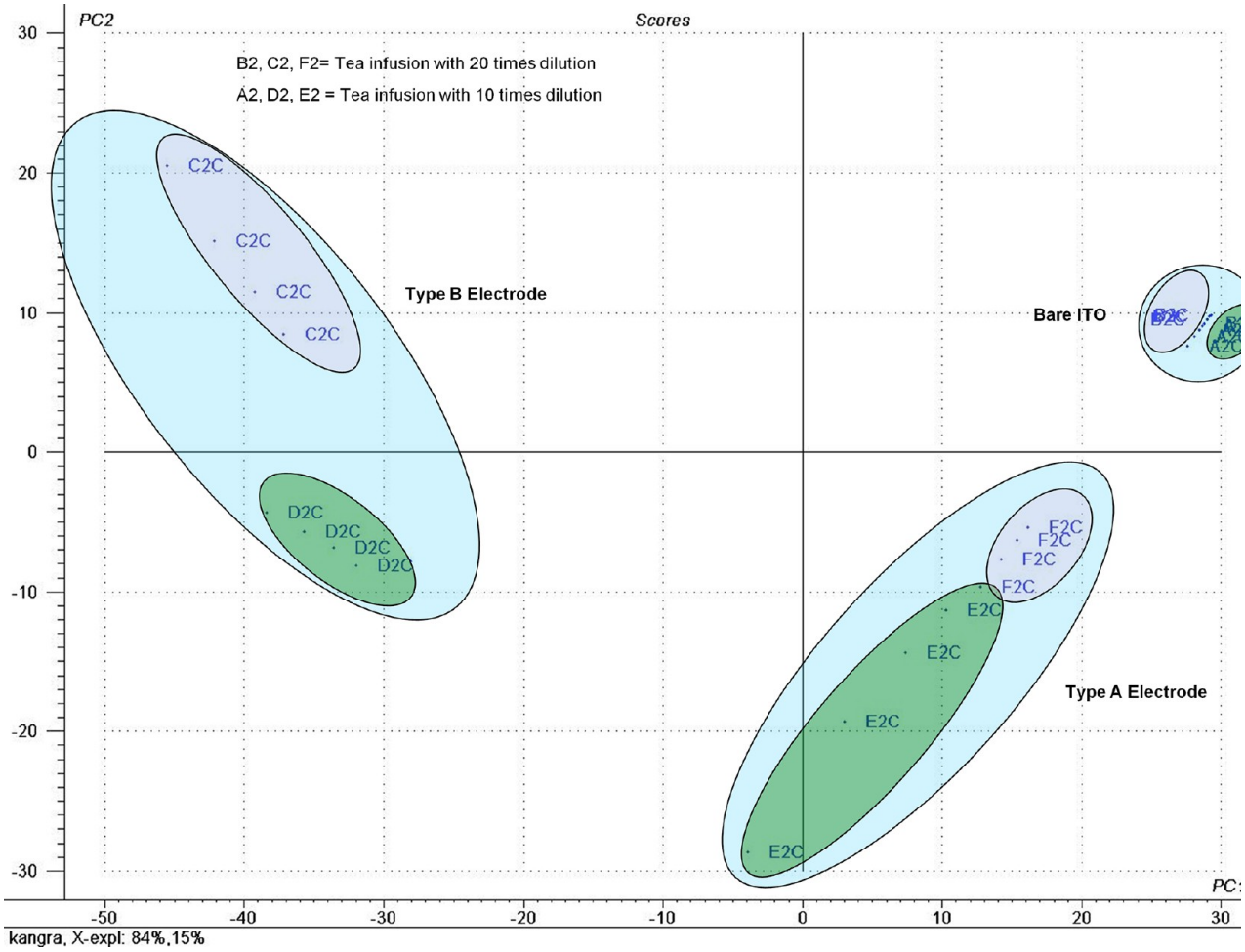

Figure 11. PCA plot of orthodox tea infusion with three types of electrodes.

peaks. However, the corresponding peaks of pure PANI at 791.2 cm^{-1} shifted to 794 cm^{-1}, 1120.7 cm^{-1} shifted to 1136 cm^{-1}, 1471.4 cm^{-1} shifted to 1490.2 cm^{-1}, and 1558.6 cm^{-1} shifted to 1580.2 cm^{-1} wave numbers in the PANI−ZnO composite. The shift may be described as due to the formation of hydrogen bonding between ZnO and the NH group of PANI on the surface of ZnO particles.

Figure 6 shows the cyclic voltammograms of catechin standards (0.1 and 0.2 mM) for type A and B electrodes, respectively.

The oxidation mechanism for catechin is known to proceed in sequential steps and is pH-dependent (Martinez et al. *J. Electroanal. Chem.* **2005**, *584*, 92−99). The oxidation of the catechol 3′,4′-dihydroxyl electron-donating groups occurs first, at very low positive potentials, and is a reversible reaction. The hydroxyl groups of the resorcinol moiety are oxidized afterward and undergo an irreversible oxidation reaction, as shown in Scheme 1.

The second step results in dimerization of the molecule forming an electroinactive species. The oxidation process involves a two electron−two proton reaction.[49] The reaction at higher pH follows a different pathway than that at lower pH, and the reaction products are easily oxidized.[50] For a pH value of 7, the first reversible oxidation of the catechol moiety is known to occur between potentials of 0 and 0.2 V.[50] The peaks in the same region of 0−0.2 V were defined by the positive/negative current maxima. This was done in order to avoid the ambiguities due to oxidation/reduction of the polymer itself in other ranges. For a type A electrode, an oxidation peak at 0.070 V is observed, whereas for a type B electrode, the peak is observed at 0.075 V. This is in agreement with the various reports on the electrochemistry of tea catechins.[51,52] The sensitivities were calculated by measuring the change in the current intensity per molar change in the concentration of the electrolyte for type A and B electrodes, i.e., $S = \Delta I_{Peak}/\Delta Conc$, where S stands for sensitivity, ΔI_{Peak} is a change in the peak current, and $\Delta Conc$ refers to a change in the concentration. The sensitivities observed at these peaks are 32 and 76 mA/M for types A and B, respectively, indicating a 2-fold increase for the type B electrode. Similarly, Figure 7 shows the cyclic voltammograms obtained for CTC and orthodox teas at two different dilutions.

It may be observed that the peaks in these voltammograms have been shifted to 0.1 V. This may be attributed to the presence of multispecies in CTC and orthodox tea samples. It may be observed that, although the current levels in type B electrodes have been reduced compared to those in type A electrodes, the relative change in the peak values in the case of type B electrodes is significantly large. For comparison, the voltammograms obtained for 0.1 and 0.2 mM catechin concentrations at the three types of electrodes are plotted in parts a and b of Figure 8, respectively. A better resolution of the catechin oxidation peak is observed at the type B electrode.

dx.doi.org/10.1021/am401257q | ACS Appl. Mater. Interfaces 2013, 5, 5346−5357

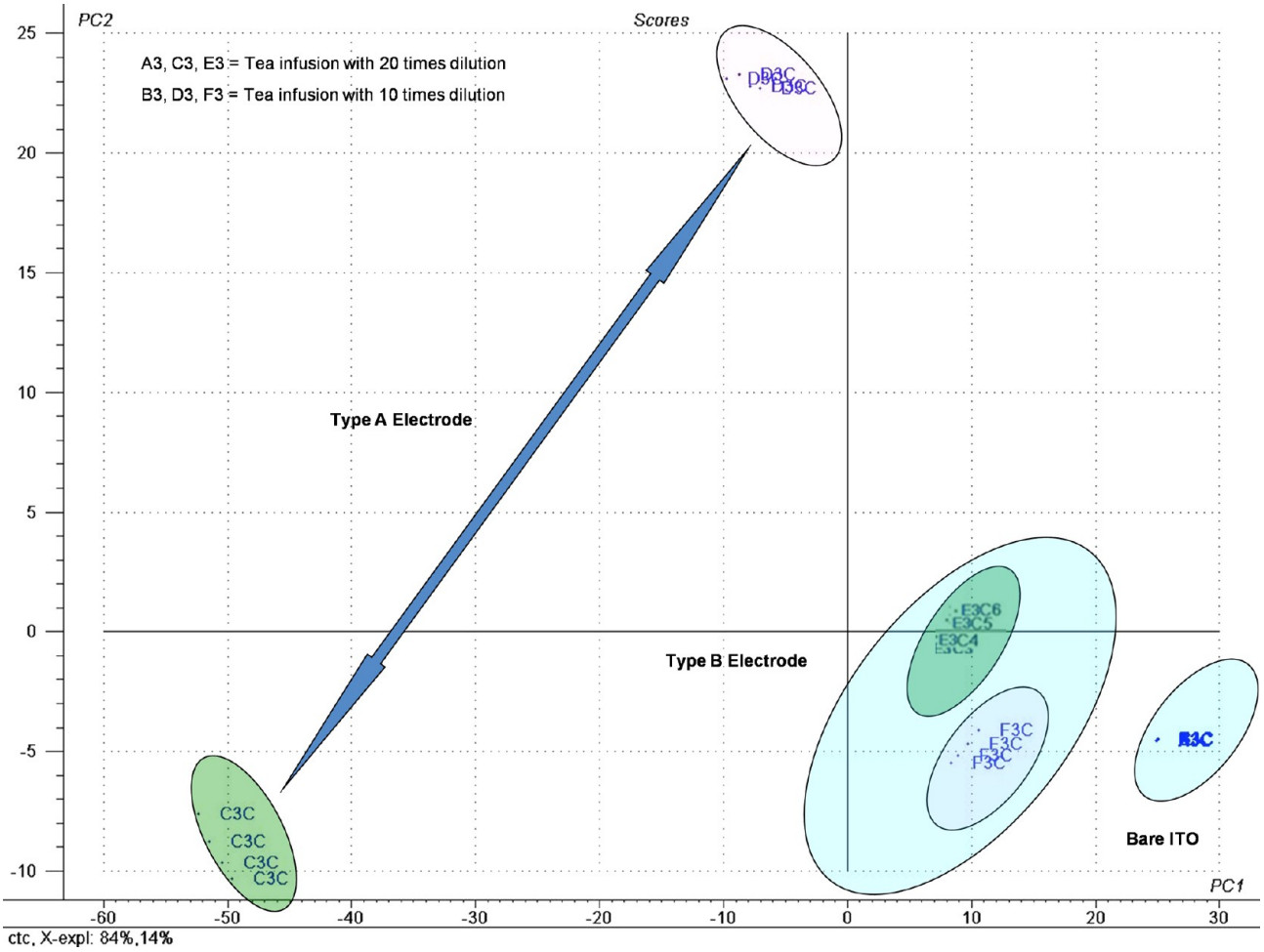

Figure 12. PCA plot of CTC tea infusion with three types of electrodes.

The charge transfer at the peak potential is a representation of the amount of polyphenols and can be used to correlate with the concentrations. On the reverse scan, the oxidized forms of the catechin/polyphenols are reduced back to the original form. The amount of current flow is governed by three factors, namely, the nature of the electrodes, the rate constant e_T, defined by the rate of electron flow from the electrolyte solution to the electrode surface and vice versa, and the temperature and mass transport of electroactive species. The mass transport or *flux* is a function of migration, convection, and diffusion. Although convection and migration do not play major roles and are not the rate-limiting factors because of high dilution, diffusion of the analyte across the solution, governed by two *Fick's laws*, is a major rate-limiting factor and is responsible for the overall reduction in the current density in the case of CTC and orthodox teas compared to the catechin sample.

The total current, i, at any location in a solution during electrolysis is given by

$$i = \frac{F^2 A}{RT}\frac{\partial \Phi}{\partial x}\sum_j z_j{}^2 D_j C_j + FA\sum_j z_j D_j \frac{\partial C_j}{\partial x}$$

for a system of cross-sectional area A. D_j is the diffusion coefficient for the electroactive species j, $\partial\Phi$ is the potential gradient along the distance ∂x, $\partial C_j/\partial x$ is the concentration gradient, and R is the gas constant at temperature T. The total current is composed of migration (first term of the above equation) and diffusion (second term of the above equation) components. The second term represents Fick's law of diffusion. In our case, the first term is assumed to be negligible due to dilution. The diffusion rate is proportional to the diffusion coefficient, which, in turn, is a function of the particle size of electroactive species, viscosity, and temperature. Therefore, the observed overall oxidation peak current densities in the case of catechin are higher compared to orthodox and CTC teas.

Figure 9 shows PCA score plots using the CV data of type A, type B, and a bare ITO electrode for the two concentrations of catechin samples. A1, C1, and E1 represent higher concentrations (0.2 mM) of catechin, whereas B1, D1, and F1 represent lower concentrations (0.1 mM) of catechin. Three major clusters for the three electrodes can be seen. The subclusters in these three major clusters represent the two sample concentrations. It may be observed that clustering is better for the type B electrode with large separation for the two concentrations compared to the type A electrode. Although two clear subclusters are also visible in the case of a bare ITO electrode but with high intraclass variance, suggesting high noise levels, there is a high degree of overlap of the two different concentration samples in the case of a type A electrode, suggesting poor discriminability or sensitivity for concentration variations. Also, because of the increase in the effective surface area of the type B electrode, the saturation

dx.doi.org/10.1021/am401257q | ACS Appl. Mater. Interfaces 2013, 5, 5346−5357

effect is minimized, thereby making type B electrodes better in terms of noise rejection, sensitivity, and activity.

To test for the possible interference effect of various biochemical species, the CV plot of standard catechin was compared with that of tea infusion whose biochemical constituents (% composition) were found by HPLC and UV−visible spectroscopy and are given in Table 1.

The CV plot of standard catechin along with tea infusion with known concentration is represented in Figure 10. A well-defined peak is observed in the case of two concentrations of catechin standard compared to the tea infusion.

In Figure 11, A2, D2, and E2 represent higher concentrations of orthodox tea infusion, whereas B2, C2, and F2 represent lower concentrations of orthodox tea infusion. The PCA plot shows that there is a drastic reduction in the intraclass variance for the type B electrode, whereas it is maximum for the type A electrode although there is a lack of proper clustering. This may be due to the fact that the type B electrode resolves the catechin oxidation peaks effectively compared to the type A electrode and the concentration of catechin in orthodox tea is more compared to CTC, in general. Figure 12 shows the PCA score plot of the CTC tea sample. A3, C3, and E3 represent higher concentrations of CTC tea infusion, whereas B3, D3, and F3 represent lower concentrations of CTC tea infusion. It is observed that the type A electrode response shows a better clustering compared to the type B electrode. This is attributed to the fact that CTC teas contain significantly less amounts of catechin. Moreover, the orthodox tea contains mainly unoxidized polyphenols of small molecular masses up to 400 amu, whereas CTC contains mainly thearubigins (TR) and theaflavins (TF), which are the oxidized products of polyphenols and have higher molecular mass. The movement of long polyphenol chains is easy in the case of the PANI fiber, where even the polyphenol molecules get ample space to be adsorbed on the surface of the PANI fibers. In the case of orthodox teas, low-molecular-weight polyphenols (catechin) can best fit onto the surface of the ZnO nanorod or the surface area between PANI fibers and ZnO nanorods. This explains the better clustering for the CTC tea samples in the case of the type A electrode and the better clustering for the orthodox tea samples in the case of the type B electrode.

5. CONCLUSION

The present work devises a novel method for the template-driven fabrication of vertically aligned ZnO nanorods at the electrochemically synthesized polyaniline surface. SEM analysis confirmed the vertical alignment and improvement in the aspect ratio of the nanorods. Further, FTIR and UV−visible spectroscopy studies confirmed the formation of the PANI−ZnO hybrid film. CV studies confirmed the improvement in the resolution of the oxidation peak and sensitivity for catechin in the PANI−ZnO hybrid film. PCA analysis confirms the discrimination ability of the hybrid film toward catechin. This work has the potential to be extended for determination of other polyphenolic compounds in the tea as well as other beverages, thus contributing toward the development of electrodes for e-tongue applications. Optimization of the developed electrodes through band-gap engineering of ZnO is envisaged in the future.

■ ASSOCIATED CONTENT

Ⓢ Supporting Information

Small sequential linear drift observed in CV plots. This material is available free of charge via the Internet at http://pubs.acs.org.

■ AUTHOR INFORMATION

Corresponding Author

*Tel: +91-172-2657811-434. Fax: +91-172-2657820. E-mail: jagvira@csio.res.in.

Notes

The authors declare no competing financial interest.

■ ACKNOWLEDGMENTS

The authors are thankful to Dr. Ashu Gulati, Scientist, CSIR-IHBT, Palampur, for providing the orthodox tea samples and her valuable guidance, Anupma Sharma, Technical Assistant, CSIR-CSIO, Gaurav Gupta, Scientist, CSIR-CSIO, Shyam Kishore, Technical Officer, for their kind help extended toward experimental work, and Dr P. K. Jain, Principal Scientist, CSIR-CSIO, for his valuable guidance and unconditional support.

■ REFERENCES

(1) Willander, M.; Nur, O.; Zhao, Q. X.; Yang, L. L.; Lorenz, M.; Cao, B. Q.; Pérez, J. Z.; Czekalla, C.; Zimmermann, G.; Grundmann, M.; Bakin, A.; Behrends, A.; Al-Suleiman, M.; El-Shaer, A.; Mofor, A. C.; Postels, B.; Waag, A.; Boukos, N.; Travlos, A.; Kwack, H. S.; Guinard, J.; Dang, D. L. S. *Nanotechnology* **2009**, *20*, 332001.

(2) Ahn, C. H.; Kim, Y. Y.; Kang, S. W.; Kong, B. H.; Mohanta, S. K.; Cho, H. K.; Kim, J. H.; Lee, H. S. *J. Mater. Sci.: Mater. Electron.* **2008**, *19*, 744−748.

(3) Huang, J. V. S.; Weiller, B. H.; Kaner, R. B. *Chem.—Eur. J.* **2004**, *10*, 1315.

(4) Arnold, M. S.; Avouris, P.; Pan, Z. W.; Wang, Z. L. *J. Phys. Chem. B* **2002**, *107*, 659−663.

(5) Huang, M. H.; Mao, S.; Feick, H.; Yan, H.; Wu, Y.; Kind, H.; Weber, E.; Russo, R.; Yang, P. *Science* **2001**, *292*, 1897−1899.

(6) Lee, C. J.; Lee, T. J.; Lyu, S. C.; Zhang, Y.; Ruh, H.; Lee, H. J. *Appl. Phys. Lett.* **2002**, *81*, 3648−3650.

(7) Wang, Z. L. *Mater. Today* **2004**, *7*, 26−33.

(8) Park, J.-H.; Choi, H.-J.; Choi, Y.-J.; Sohn, S.-H.; Park, J.-G. *J. Mater. Chem.* **2004**, *14*, 35−36.

(9) Park, J.-H.; Choi, H.-J.; Park, J.-G. *J. Cryst. Growth* **2004**, *263*, 237−242.

(10) Wang, G.; Lu, W.; Li, J.; Choi, J.; Jeong, Y.; Choi, S.-Y.; Park, J.-B.; Ryu, M. K.; Lee, K. *Small* **2006**, *2*, 1436−1439.

(11) Wang, G.; Wang, Q.; Lu, W.; Li, J. *J. Phys. Chem. B* **2006**, *110*, 22029−22034.

(12) Yau, W.-H.; Tseng, P.-C.; Lian, D. *Nucl. Instrum. Methods Phys. Res., Sect. B* **2011**, *269*, 1450−1454.

(13) Kang, T.-T.; Liu, X.; Zhang, R. Q.; Hu, W. G.; Cong, G.; Zhao, F.-A.; Zhu, Q. *Appl. Phys. Lett.* **2006**, *89*, 071113−3.

(14) Breedon, M.; Rahmani, M. B.; Keshmiri, S.-H.; Wlodarski, W.; Kalantar-zadeh, K. *Mater. Lett.* **2010**, *64*, 291−294.

(15) Ng, H. T.; Li, J.; Smith, M. K.; Nguyen, P.; Cassell, A.; Han, J.; Meyyappan, M. *Science* **2003**, *300*, 1249.

(16) Charu, D.; Dutta, V. *Adv. Nat. Sci.: Nanosci. Nanotechnol.* **2012**, *3*, 015011.

(17) Sun, Y.; Fuge, G. M.; Fox, N. A.; Riley, D. J.; Ashfold, M. N. R. *Adv. Mater.* **2005**, *17*, 2477−2481.

(18) Kim, K. S.; Jeong, H.; Jeong, M. S.; Jung, G. Y. *Adv. Funct. Mater.* **2010**, *20*, 3055−3063.

(19) Tam, N.-D.; Karandeep, S.; Meyyappan, M.; Michael, M. O. *Nanotechnology* **2012**, *23*, 194015.

(20) Elias, J.; Lévy-Clément, C.; Bechelany, M.; Michler, J.; Wang, G.-Y.; Wang, Z.; Philippe, L. *Adv. Mater.* **2010**, *22*, 1607−1612.

(21) Kumar, V.; Kumar, S.; Chakarvarti, S. K. *J. Mater. Sci.: Mater. Electron.* **2010**, *21*, 1277−1280.
(22) Sharma, A.; Bhondekar, A. P.; Bari, S. S.; Gulati, A.; Kapur, P.; Singla, M. L. *J. Liq. Chromatogr. Relat. Technol.* **2011**, *34*, 2243−2255.
(23) Dutta, R.; Hines, E. L.; Gardner, J. W.; Kashwan, K. R.; Bhuyan, M. *Sens. Actuators, B* **2003**, *94*, 228−237.
(24) Lozano, J.; Santos, J. P.; Aleixandre, M.; Sayago, I.; Gutierrez, J.; Horrillo, M. C. *IEEE Sens. J.* **2006**, *6*, 173−178.
(25) Bhattacharyya, N.; Bandyopadhyay, R.; Bhuyan, M.; Tudu, B.; Ghosh, D.; Jana, A. *IEEE Trans. Instrum. Meas.* **2008**, *57*, 1313−1321.
(26) Bhattacharyya, N.; Seth, S.; Tudu, B.; Tamuly, P.; Jana, A.; Ghosh, D.; Bandyopadhyay, R.; Bhuyan, M. *J. Food Eng.* **2007**, *80*, 1146−1156.
(27) Dutta, R.; Kashwan, K. R.; Bhuyan, M.; Hines, E. L.; Gardner, J. W. *Int. Jt. Conf. Neural Networks, Proc.* **2003**, *16*, 847−853.
(28) Furuno, K.; Akasako, T.; Sugihara, N. *Biol. Pharm. Bull.* **2002**, *25* (1), 19−23.
(29) Yang, B.; Kotani, A.; Arai, K.; Kusu, F. *Anal. Sci.* **2001**, *17* (5), 599−604.
(30) John, R.; Wallace, G. G. *J. Electroanal. Chem.* **1993**, *354*, 145−160.
(31) Tang, C.-F.; Kumar, S. A.; Chen, S.-M. *Anal. Biochem.* **2008**, *380*, 174−183.
(32) Ramos, L. S.; Beebe, K. R.; Carey, W. P.; Sanchez, E.; Erickson, B. C.; Wilson, B. E.; Wangen, L. E.; Kowalski, B. R. *Anal. Chem.* **1986**, *58*, 294R−315R.
(33) Ballantine, D. S.; Rose, S. L.; Grate, J. W.; Wohltjen, H. *Anal. Chem.* **1986**, *58*, 3058−3066.
(34) Kumar, R.; Bhondekar, A. P.; Kaur, R.; Vig, S.; Sharma, A.; Kapur, P. *Sens. Actuators, B* **2012**, *171−172*, 1046−1053.
(35) Bhondekar, A. P.; Dhiman, M.; Sharma, A.; Bhakta, A.; Ganguli, A.; Bari, S. S.; Vig, R.; Kapur, P.; Singla, M. L. *Sens. Actuators, B* **2010**, *148*, 601−609.
(36) Bhondekar, A. P.; Kaur, R.; Kumar, R.; Vig, R.; Kapur, P. *Chemom. Intell. Lab. Syst.* **2011**, *109*, 65−76.
(37) Bhondekar, A. P.; Vig, R.; Gulati, A.; Singla, M. L.; Kapur, P. *IEEE Sens. J.* **2011**, *11*, 3462−3468.
(38) Li, Y.; Gong, J.; McCune, M.; He, G.; Deng, Y. *Synth. Met.* **2010**, *160*, 499−503.
(39) Xu, H.; Chen, X.; Zhang, J.; Wang, J.; Cao, B.; Cui, D. *Sens. Actuators, B* **2012**.
(40) Lifshitz, I. M.; Slyozov, V. V. *J. Phys. Chem. Solids* **1961**, *19*, 35−50.
(41) Wagner, C. *Z. Elektrochem., Ber. Bunsenges. Physikal. Chem.* **1961**, *65*, 581−591.
(42) Qu, L.; Yu, W. W.; Peng, X. *Nano Lett.* **2004**, *4*, 465−469.
(43) Oskam, G.; Nellore, A.; Penn, R. L.; Searson, P. C. *J. Phys. Chem. B* **2003**, *107*, 1734−1738.
(44) Mohamed, M. B.; Wang, Z. L.; El-Sayed, M. A. *J. Phys. Chem. A* **1999**, *103*, 10255−10259.
(45) Talapin, D. V.; Rogach, A. L.; Haase, M.; Weller, H. *J. Phys. Chem. B* **2001**, *105*, 12278−12285.
(46) Kar, S.; Dev, A.; Chaudhuri, S. *J. Phys. Chem. B* **2006**, *110*, 17848−17853.
(47) Gaikwad, P. D.; Shirale, D. J.; Gade, V. K.; Savale, P. A.; Kharat, H. J.; Kakde, K. P.; Shirsat, M. D. *Int. J. Electrochem. Sci.* **2006**, *1*, 425−434.
(48) Xu, J. C.; Liu, W. M.; Li, H. L. *Mater. Sci. Eng., C* **2005** *25*.
(49) Vestergaard, M. d.; Kerman, K.; Tamiya, E. *Anal. Chim. Acta* **2005**, *538*, 273−281.
(50) Janeiro, P.; Oliveira Brett, A. M. *Anal. Chim. Acta* **2004**, *518*, 109−115.
(51) Kondo, K.; Kurihara, M.; Fukuhara, K.; Lester, P. Mechanism of antioxidant effect of catechins. *Methods in Enzymology*; Academic Press: New York, 2001; Vol. *335*, pp 203−217.
(52) Yang, B.; Kotani, A.; Arai, K.; Kusu, F. *Chem. Pharm. Bull.* **2001**, *49*, 747−751.